Physics – Uspekhi **69** (3) 222 – 230 (2026)

CONFERENCES AND SYMPOSIA

PACS numbers: **95.35. + d, 95.36. + x, 98.65. – r**

Problems of cosmology on small scales of the Universe *

I.D. Karachentsev

DOI: https://doi.org/10.3367/UFNe.2025.03.039964

Contents

Abstract. Six challenges for the standard cosmological model ΛCDM are listed, which arise when comparing theoretical predictions with observational data on scales of ~ 1 Mpc. Different parameters of luminous and dwarf galaxies in the local sphere with a radius of 12 Mpc are presented. The average densities of stellar matter and dark matter are reproduced depending on a distance in the Local volume. Observational data on distribution of angular momentum of nearby galaxies are considered. A comparison of the dark matter mass estimates for systems of galaxies based on motions of their internal (virialized) members and neighboring galaxies is given. The reasons for the low derived value of the matter density, $\Omega_{\rm m} = 0.08 \pm 0.02$, in the Local Universe with respect to the global value $\Omega_{\rm m} = 0.30 \pm 0.02$ are discussed.

Keywords: galaxies, dark matter, systems of galaxies

1. Introduction

The standard cosmological model (ΛCDM), with a relative density of baryonic matter of $\Omega_{\rm b} = 0.04$, cold dark matter density of $\Omega_{\rm DM} = 0.26$, and a dominant dark energy component of $\Omega_\Lambda = 0.70$, successfully describes the observed structure of the Universe on large scales. Results from numerical (N-body) simulations of the formation and evolution of large-scale structure convincingly show that it represents a cosmic 'web,' where galaxies are concentrated in 'walls,' at the intersections of which extended filaments (chains of galaxies) form. In turn, at the intersections of cosmic filaments, massive knots — galaxy clusters — form, with their populations being replenished by the influx of new galaxies along the filaments. As galaxies move relative to each other in dense regions of clusters, their light gas components are stripped and collectivized, leading to the formation of a hot gas intracluster medium that emits strongly in X-rays. The bulk of the Universe is occupied by cosmic voids framed by walls and filaments. Dwarf galaxies, rich in gas and actively forming stars, are occasionally found in these voids.

All these elements of a large-scale structure are presented in Fig. 1, which shows the distribution of 5000 nearby galaxies with radial velocities less than 1500 km s^{-1} across the sky at equatorial coordinates. At the center of this map is the Virgo Cluster, whose virial region is indicated by a black circle. The Virgo Cluster, located at a distance of 16 megaparsecs (Mpc), is adjacent to cosmic filaments, forming a starfish pattern. A vast void (the Local Void) is visible on the left side of the figure, with an angular size of up to one radian. The Local Void begins at the boundary of the Local Group of galaxies and extends to a distance of approximately 20 Mpc. Galaxies with active and quenched star formation are color-coded according to their morphological type on the de Vaucouleurs numerical scale, shown in the upper left corner of the figure. The figure clearly demonstrates that gas-rich galaxies with young stellar populations predominate in low-density regions, while the Virgo and Fornax Clusters (located in the lower right part of the figure) are dominated by galaxies with old stellar populations, embedded in a massive, hot gas environment. Through X-ray 'lenses,' only the two marked clusters would be visible on this map against a generally dark background. The various properties of galaxy clusters and their role in cosmology are discussed in detail in the review by Vikhlinin et al. [1].

I.D. Karachentsev
Special Astrophysical Observatory, Russian Academy of Sciences, Nizhnii Arkhyz, Zelenchukskiy region, Karachai-Cherkessian Republic, Russian Federation
E-mail: idkarach@gmail.com

Received 2 April 2025
Uspekhi Fizicheskikh Nauk **196** (3) 239 – 247 (2026)
Translated by I.A. Ulitkin

* This review is based on the report presented for the Scientific Session of the Physical Sciences Division of the Russian Academy of Sciences (PSD RAS), on March 19, 2025 (see *Physics–Uspekhi* **69** (3) 221 (2026); *Uspekhi Fizicheskikh Nauk* **196** (3) 238 (2025)).

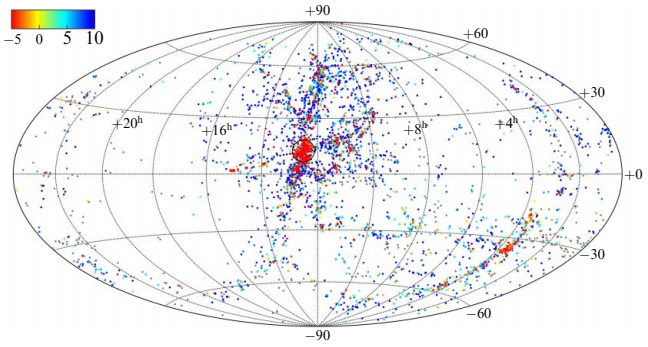

Figure 1. Sky distribution of 5000 nearby galaxies with radial velocities less than 1500 km s^{-1} in equatorial coordinates. Galaxies of different morphological types on the numerical scale (top left) are shown in different colors. The virial region of the Virgo cluster is marked by a circle.

2. Challenges for the standard cosmological model

With increasing computational resources used for N-body simulations of the dynamical evolution of the Universe, the spatial resolution of cosmic structures has reached a scale of ~ 1 Mpc, or a galaxy mass resolution of about 10^7 solar masses [2–4]. However, significant discrepancies have arisen between simulation results and observational data. Overcoming these discrepancies is an important incentive for improving the standard cosmological model. Below, we summarize six main discrepancies discussed in the literature.

2.1 Lack of dwarf satellites for massive galaxies

Model calculations yield a rather steep power-law mass spectrum for dark matter halos in which baryons accumulate and subsequently form galaxies [5, 6]. The observed number of small satellites around massive galaxies such as the Milky Way and the Andromeda Galaxy turned out to be tens of times smaller than that predicted by ΛCDM models. Observational astronomers have conducted systematic searches for new dwarf satellites using modern deep sky surveys across various spectral ranges, which has partially alleviated this discrepancy. On the other hand, theorists have taken into account that, during their evolution, a significant fraction of satellites disappeared, being absorbed by larger galaxies due to dynamical friction [7]. Currently, this discrepancy persists, although in a less acute form.

2.2 Excess of thin coplanar structures among satellites

Over the past decade, numerous publications have appeared indicating that the satellites of massive galaxies are not distributed chaotically in space, but instead form thin, planar structures with coherent satellite motion [8–11]. In particular, such coplanar subsystems have been discovered in satellites of the Milky Way, the Andromeda Galaxy (M31), and other nearby massive galaxies. The characteristic thickness of flat satellite systems was found to be approximately 20 kpc, with a total radial extent of 200 kpc. The probability of detecting such structures based on numerical simulations was found to be very low. This problem remains unresolved, although newly discovered satellites are not always embedded in known planar structures. One possible explanation for the presence of thin coplanar structures among satellites could be anisotropic accretion of nearby dwarfs, which are concentrated in cosmic filaments, onto a massive hosts [12].

2.3 Discrepancy between Hubble parameter estimates

According to data from the Planck mission, the global value of the Hubble parameter, which determines the expansion rate of the Universe and its age, is $H_0 = (67 \pm 1)\,\mathrm{km\,s^{-1}\,Mpc^{-1}}$ [13, 14]. In contrast, the local value of the Hubble parameter, obtained from a comparison of radial velocities and distances of galaxies, $H_0 = (74 \pm 2)$ km s^{-1} Mpc^{-1} [15–17], significantly exceeds the global value. This discrepancy between the H_0 estimates is commonly referred to as the 'Hubble tension.' The local value of the H_0 parameter is determined on scales of ~ 100 Mpc. When measuring it, it is necessary to carefully take into account cosmic flows, the amplitudes of which in different parts of the sky can reach several hundred km s^{-1}. For example, our Galaxy has an individual velocity of about 630 km s^{-1} relative to the cosmic microwave background radiation. Nevertheless, taking into account local flows and uncertainties at the zero point of the distance scale, the difference between the local and global values of the H_0 parameter significantly exceeds the errors in their measurement. To explain this contradiction, it was suggested that an observer on the Earth is located in the middle of a huge cosmic gap measuring $\sim (200-300)$ Mpc [18, 19]. According to numerical simulations, the voids expand at a rate approximately 10–15% higher than the global rate. Therefore, an observer located near the void's center could explain the higher expansion rate of the local region of the Universe. However, the standard cosmological model does not predict average matter density fluctuations with an amplitude greater than 3% on scales greater than 200 Mpc.

2.4 Lost baryon problem

The baryon-to-dark matter ratio of in the ΛCDM model is Ω_b: $\Omega_{DM} \simeq 1:6$. However, the observed ratio of light (stellar) to dark matter densities, Ω_*:$\Omega_{DM} \simeq 1:42$, is approximately seven times smaller than the expected one [20, 21]. In rich galaxy clusters, the mass of hot gas exceeds the total mass of stars by an order of magnitude [1, 22]. Accounting for the ionized gas of clusters weakens the problem of missing baryons; however, a discrepancy at the level of a factor of 2–3 still remains. In recent years, a new tool has emerged for probing the intergalactic medium via dispersion measures and redshift in fast radio bursts (FRBs). This method allows one to estimate the average density of free electrons along the line of sight [23]. Data obtained from studying FRBs have shown that the intergalactic space is filled with warm ionized gas, the temperature of which is too low to be detected in the X-ray range. The average density of this medium turned out to be quite sufficient to resolve the missing baryon problem [24, 25].

2.5 Problem of missing dark matter

The issue of the existence of dark matter in and between galaxies has a nearly 90-year history [26]. Observational manifestations of dark matter are visible in flat (nondecreasing, non-Keplerian) rotation curves at the outskirts of galaxies, as well as in the large dispersion of radial velocities in galaxies in groups and clusters. The physical nature of dark matter remains unknown. A detailed review of observational data indicating the presence of nonbaryonic dark matter is presented in [27]. The ratio of dark to light (stellar) matter increases from normal galaxies toward dwarf galaxies and from binary and triple systems toward rich groups and clusters. The minimum of this ratio occurs in massive galaxies such as the Milky Way. Most estimates

of the dark matter mass in galaxy groups and clusters are based on the application of the virial theorem, which assumes a balance between the kinetic (T) and potential (U) energies of a system of gravitating bodies: $2T + U = 0$. If the system contains a central dominant galaxy, its total mass is estimated from the orbital motions of its small satellites. Recently, new and independent estimates of the total cluster mass have appeared using the weak gravitational lensing effect, based on an analysis of the pattern of position angles of distant galaxies around a nearby cluster with a known redshift. In general, the agreement between the mass estimates obtained by both methods is quite satisfactory [28, 29].

Collection of nearby groups and clusters covering the entire sky and the application of virial mass estimates to them have shown that the average density of matter contained in galaxy systems of different scales is $\Omega_{\rm m} = 0.08 \pm 0.02$ [30–33]. This density is clearly insufficient to reconcile it with the global value $\Omega_{\rm m} = 0.30 \pm 0.02$ [12, 13], which follows from an analysis of the properties of the cosmic microwave background radiation. It is natural to assume that the missing portion of dark matter is distributed among groups and clusters of galaxies, but direct methods for its detection have not yet been proposed. The discussion of this most important and complex problem will be continued in Section 5.

2.6 Discrepancy between the expected and observed orientations of galaxy spins

The angular momentum of the galaxy rotation, its spin, is a highly conservative characteristic, remaining constant in magnitude and direction throughout cosmological time. For this reason, angular momenta are important indicators of the initial conditions of galaxy formation. According to theoretical predictions, the spin directions of galaxies are oriented predominantly in the plane of the wall in which they are located [34–36]. In particular, galaxies in the Local Supercluster are expected to show alignment of their spins along the supercluster equator. However, attempts to test this prediction have not yet revealed any significant preference in spin orientation [37, 38].

3. Representative sample of galaxies in the Local volume

Catalogs of stars and galaxies are usually compiled by restricting the sample of objects by their apparent magnitude (flux). The large-scale structure of the Universe is simulated numerically within a finite volume of space. Therefore, the results of cosmological simulations are verified using a sample of galaxies limited by a fixed distance. Compiling such a sample is associated with great difficulties due to the enormous range of luminosities of galaxies, as well as the uncertainties in their distance measurements. For example, the list of the 1000 brightest galaxies overlaps the list of the nearest galaxies by less than 10%. The first list of the Milky Way's neighbors was compiled in 1979 [39] and included only 179 galaxies with distances less than 10 Mpc of the observer. Over the years, thanks to targeted efforts [40, 41], the sample of nearby galaxies has been increased by almost an order of magnitude. This list continues to be expanded at the present time, mainly due to the discovery of increasingly faint, low-surface-brightness galaxies with. The creation of a model and a representative sample of galaxies in the Local volume consisted of several main stages.

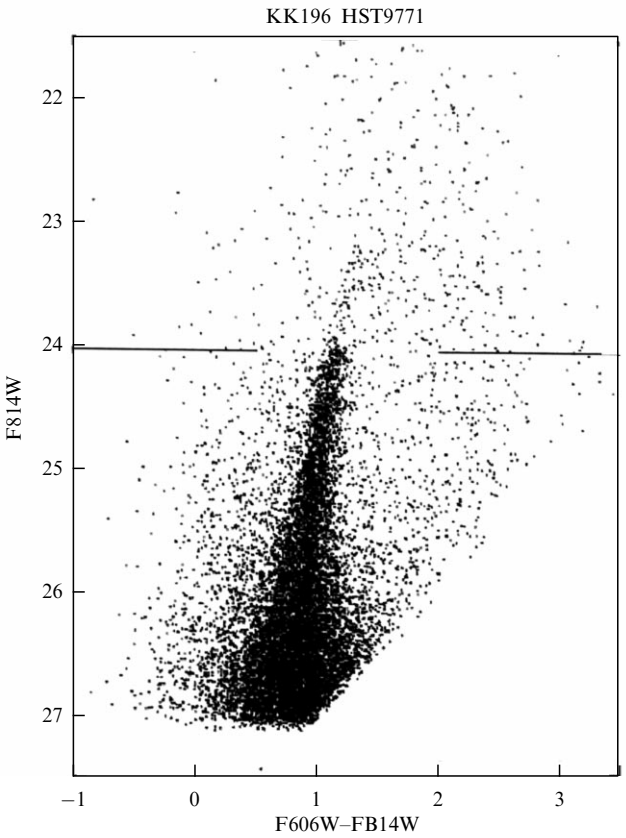

Figure 2. Color–magnitude diagram for stars in the dwarf galaxy KK196 at a distance of 3.96 Mpc, obtained from images in the F814W and F606W filters taken with the Hubble Space Telescope. The position of the tip of the red giant branch is indicated by a horizontal line.

1. To search for new nearby low-luminosity galaxies, large-scale surveys of the northern and southern skies were used in the optical range (POSS-II, ESO SERC, SDSS, DESI [42, 43]) and in the 21-cm neutral hydrogen radio line (HIPASS, Arecibo survey, FAST survey [44–46]).

2. Large-scale measurements of the radial velocities of selected candidate nearby galaxies were carried out using the 6-meter optical telescope (BTA) of the Russian Academy of Sciences [47], the 100-m radio telescope in Effelsberg, Germany [48–50], and other major radio telescopes.

3. The distances to galaxies were determined using the Hubble Space Telescope (HST) based on the luminosity of the tip of the red giant branch (TRGB). Using images of the galaxy in two filters, a color-magnitude diagram for the stars was constructed. The TRGB position, determined by the parameters of nuclear reactions in the star interior, made it possible to measure the distance of any type of galaxy with an accuracy of $\sim 5\%$. As an example, Fig. 2 shows the color-magnitude diagram for the dwarf galaxy KK196, located at a distance of 3.96 Mpc. In total, high-precision distances for more than 500 nearby galaxies were measured using images obtained with the HST.

4. For Local volume galaxies with distances within 12 Mpc, the integrated luminosities, stellar and gaseous component masses, star formation rates, and other characteristics were determined. A catalog and atlas of ~ 1700 Local volume galaxies is presented in the database [51], which is periodically updated with new objects, while the basic parameters of the galaxies are continuously refined. As the title page of the

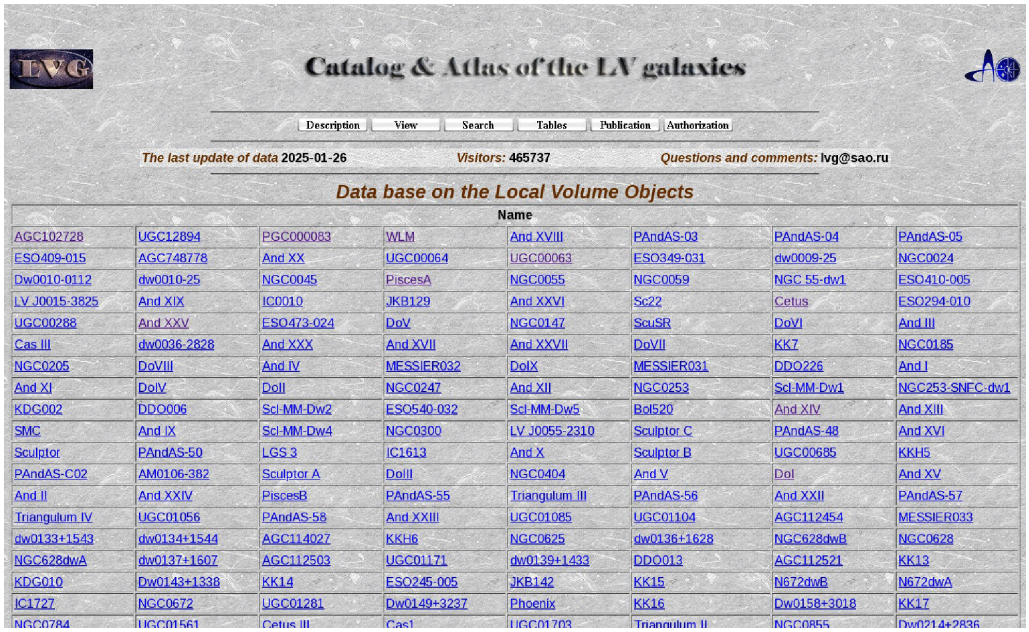

Figure 3. Front page of the Local Volume Galaxy Database. As of January 26, 2025, the number of database visits was 465737.

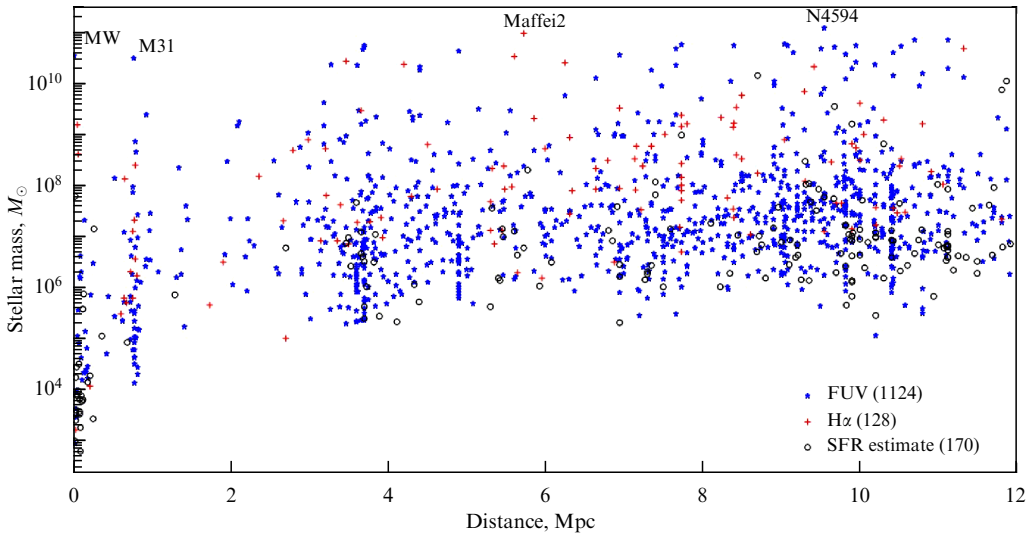

Figure 4. Distribution of local volume galaxies by stellar mass (in solar-mass units) and distance (in Mpc). Different symbols denote galaxies whose star formation rate determined by far-ultraviolet flux (FUV), Hα flux, and the mass-to-SFR calibration relation.

database (Fig. 3) shows, the number of visits has already exceeded 400,000, and the number of citations of the two published versions of the catalog [40, 41] has reached 1300.

Figure 4 shows the distribution of Local volume galaxies by stellar mass and distance from the observer. Within a distance of 12 Mpc, there are 27 galaxies with stellar masses comparable to the Milky Way (MW) and the Andromeda Nebula (M31). About half of all fainter galaxies are associated with these giants. The spread of galaxies in stellar mass reaches six orders of magnitude. Measurements of the difference in radial velocities (ΔV) of the companion galaxies and their projected separations (R_p) relative to the main galaxy allow the total dynamical mass of the group to be determined [52]

$$M_\mathrm{T} = \left(\frac{16\pi}{G}\right)\langle \Delta V^2 R_\mathrm{p}\rangle\,,$$

where G is the gravitational constant. Here, the assumption is made that the orbits of the satellites are oriented randomly relative to the line of sight, and their average orbital eccentricity is $\langle e^2\rangle = 1/2$, as follows from the results of numerical simulations of galaxies in the standard cosmological model.

Table 1 presents a list of the 27 most massive galaxies in the Local volume. Its columns indicate: (1) the galaxy name, (2) its distance from the observer in Mpc, (3) the number of satellites with measured radial velocities, (4) the dispersion of the radial velocities of the satellites, (5) the integrated mass of the group, and (6) the ratio of the integrated mass to the stellar mass of the group. As follows from these data, typical velocities of galaxy motion in nearby groups are ~ 100 km s^{-1}, and the typical ratio of the total mass to the stellar mass is characterized by a value of $M_\mathrm{T}/M_* \sim 40$.

Table 1. The most massive galaxies of the Local Volume.

Name	D	N_v	σ_v	$M_{\rm T}$	$M_{\rm T}/M_*$
	Mpc		km s^{-1}	$10^{12}/M_\odot$	
Milky Way	0.01	45	109	1.17	38 ± 13
M31	0.77	51	113	1.70	48 ± 9
NGC253	3.70	7	42	0.81	13 ± 4
N628 = M74	10.19	9	69	1.44	60 ± 22
NGC891	9.95	5	92	0.83	14 ± 3
NGC1291	9.08	2	121	4.35	75 ± 7
IC342	3.28	8	73	1.59	58 ± 29
NGC2683	9.82	2	43	0.12	3 ± 3
NGC2784	9.82	2	111	3.04	80 ± 80
NGC2903	9.17	5	41	0.45	11 ± 9
N3031 = M81	3.70	31	123	3.10	37 ± 10
NGC3115	10.20	10	112	4.82	80 ± 25
NGC3184	11.12	2	59	0.66	33 ± 4
N3379 = M105	10.80	33	136	5.75	30 ± 7
NGC3521	10.70	3	55	0.89	12 ± 5
N3556 = M108	9.90	2	67	1.07	52 ± 47
N3627 = M66	11.10	22	135	5.89	6 ± 6
NGC4258	7.66	11	96	2.09	39 ± 18
Sombrero	9.55	15	96	13.38	91 ± 35
N4736 = M94	4.41	15	68	2.40	83 ± 28
N5055 = M63	9.04	7	54	0.51	8 ± 3
NGC5128	3.68	34	124	4.67	58 ± 17
N5194 = M51	8.40	5	83	1.35	17 ± 14
NGC5236	4.90	10	61	1.07	24 ± 6
N5457 = M101	6.95	8	69	1.07	27 ± 10
NGC6744	9.51	5	71	1.55	24 ± 14
NGC6946	7.73	8	65	1.23	20 ± 8

4. Orientation of galaxy spins in the Local volume

The absolute value of the angular momentum of a galaxy, defined as the product of the amplitude of its disk rotation by the characteristic radius of the disk and its baryonic mass, varies over more than nine orders of magnitude depending on the luminosity of the galaxy and its morphological type. For a galaxy arbitrarily oriented relative to the line of sight, the spatial direction of its spin can be determined by identifying, from spectral data, which side of its disk is moving away from the observer. In this case, it is necessary to determine which side along the minor axis of the galaxy image is closer to the observer. These conditions can only be met for the nearest large galaxies, where detailed structure is discernible. In more distant regions, beyond the Local volume, samples of galaxies oriented edge-on [37, 53] or face-on, where the direction of the spiral pattern twist (clockwise or counter-clockwise) can be identified [54], are used to analyze the spin orientation. As a result, weak signs of anisotropy in the spin distribution of spiral galaxies have been detected. However, questions remained as to whether the observed anisotropy was related to the location of the galaxies relative to the nearest walls and filaments of the large-scale structure. Therefore, we examined the spin orientation of the galaxies in the Local volume, where the effects of observational selection and sample incompleteness are minimal, and the plane of the Local Wall, coinciding with the plane of the Local Supercluster, is clearly visible.

For each of the 27 major galaxies in the Local volume, the magnitude and direction of the angular momentum were determined [38]. The remaining smaller galaxies posess small angular momenta; the contribution of their absolute angular momenta to the total sum does not exceed 10%. The spin orientation of the 27 major galaxies on the celestial sphere is shown in Fig. 5 in supergalactic coordinates based on the data from [38]. The uncertainty in determining the spin direction is $\sim 5°$. The size of the circle in the figure is proportional to the logarithm of the angular momentum. The distribution of spin directions does not reveal any preferential alignment toward the plane of the Local Supercluster (SGB $\simeq 0$), as predicted by the standard ΛCDM model. Moreover, the average deviation of galaxies from the plane of the Local Supercluster does not exceed ± 2 Mpc (the SGZ scale in Fig. 5). Thus, we can conclude that, on a scale of 12 Mpc, the orientation of galaxy spins appears largely chaotic.

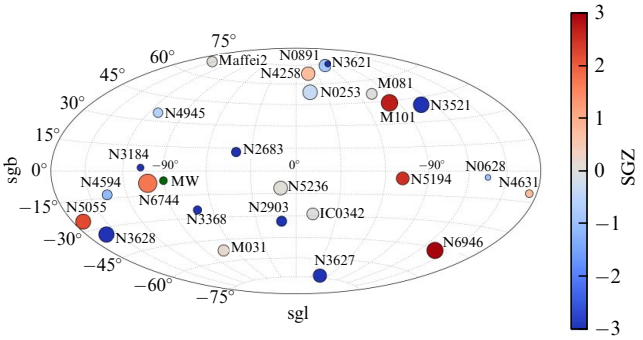

Figure 5. Distribution of spin directions of the largest nearby galaxies on the sky in supergalactic coordinates. The size of the circle is proportional to the logarithm of the absolute value of the angular momentum. The scale on the right reflects the galaxy position relative to the plane of the local 'wall' in Mpc.

5. Local Hubble flow of galaxies, dark matter, and dark energy

The total mass of a group or cluster of galaxies can be determined not only from the internal (virial) motions of the group/cluster members, but also from the motions of external (neighboring) galaxies. Figure 6 shows the distribution of the nearest galaxies by distance from the dynamic center of the Local Group (located at a distance of 0.45 Mpc from the Milky Way in the direction of the Andromeda Galaxy) and their velocity relative to the center of the Local Group. The vertical cloud on the left side of the figure is formed by satellites of the Milky Way and Andromeda with virial velocities of ~ 100 km s^{-1}. Neighboring galaxies with distances $D > 1$ Mpc have positive radial velocities, participating in the general cosmological expansion. The dotted sloping line in the figure corresponds to the unperturbed Hubble flow. The gravitational influence of the Local Group slows down the motion of neighboring galaxies. The regression line drawn along them intersects the zero-velocity level at $R_0 \simeq 1$ Mpc. This is the radius of the 'zero velocity sphere,' which separates the collapsing region around the Local Group from the general cosmological expansion. The typical ratio of R_0 to the virial radius of the group is $R_0/R_v \simeq 3.5$. For a fixed value of the parameter Ω_Λ, the total mass of the attractor (group or cluster) is related to R_0 by the expression

$$M_T(R_0) = \left(\frac{\pi^2}{8G}\right) H_0^2 C(\Omega_\Lambda) R_0^3,$$

where $C(\Omega_\Lambda)$ is a dimensionless factor ranging from 1 to 9/4. For $\Omega_\Lambda = 0.7$ and $H_0 = 74$ km s^{-1} Mpc^{-1}, this expression takes the form $M_T/M_\odot = 2.1 \times 10^{12}(R_0/\mathrm{Mpc})^3$.

We have determined the radius R_0 for the Local Group [55], for a synthetic group composed of several neighboring groups [56], and for the nearby rich Virgo cluster [57, 58]. The results are presented in Table 2. As follows from these data, the estimates of the total mass of the groups and clusters derived from the virial motions of the members (M_v) agree with the mass estimates from the motions of neighboring galaxies $M(R_0)$ within the statistical errors of both methods. Note, however, that the relatively low error in estimating the mass of the Local Group from the radius R_0 is due to the small dispersion of the radial velocities of galaxies in the neighboring Hubble flow. According to the latest data [59], the observed dispersion of the radial velocities of galaxies falling toward the Local Group is only 15 km s^{-1}, which is significantly less than the value of 70 km s^{-1} obtained from numerical simulations of the local flow. This discrepancy can be regarded as another small-scale challenge for the standard cosmological model.

Table 2. Estimated total mass of galaxy systems.

Systems	$M_v/M_\odot$	$M(R_0)/M_\odot$	R_0/Mpc
Local group	$(2.8 \pm 0.6) \times 10^{12}$	$(1.9 \pm 0.2) \times 10^{12}$	0.96 ± 0.03
Synthetic group	$(1.8 \pm 0.5) \times 10^{12}$	$(1.7 \pm 0.2) \times 10^{12}$	0.93 ± 0.03
Virgo Cluster	$(6.3 \pm 0.9) \times 10^{14}$	$(7.2 \pm 0.9) \times 10^{14}$	7.0 ± 0.2

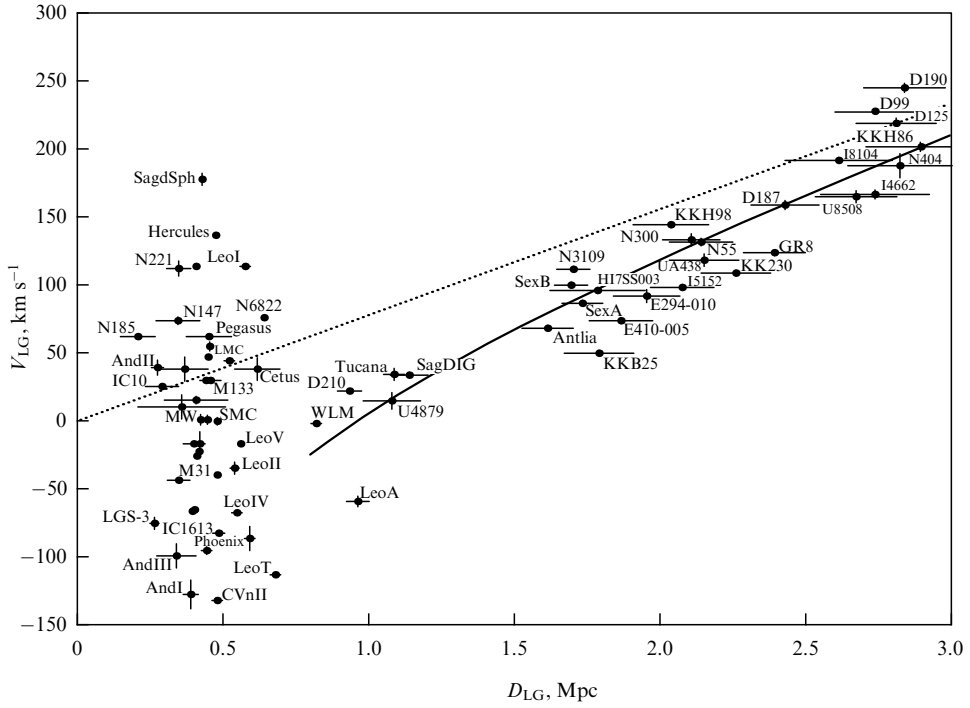

Figure 6. Radial velocities and distances of the nearest galaxies relative to the center of mass of the Local Group. Members of the Local Group form a vertical cloud on the left side of the diagram with virial velocities of approximately 100 km s^{-1}. The slanted dotted line depicts the ideal unperturbed Hubble flow. Galaxies surrounding the Local Group participate in the general cosmological expansion, but their velocities are slowed by the gravitational influence of the Local Group.

The agreement between the mass values in volumes $(R_v)^3$ and $(3.5R_v)^3$ indicates that the bulk of the dark matter mass is concentrated within the virial radius of galaxy systems. Note also that the kinematics of the Hubble flow depends on the magnitude of the Λ term, which acts as a universal repulsive force between galaxies. Furthermore, assuming the absence of the Λ term would lead to paradoxical mass estimates within $3.5R_v$ that are smaller than those within R_v. Here we have observational evidence of dark energy acting at close distances, which is important because the evidence for the dark energy came from observations of extremely distant events — supernova explosions that occurred billions of years ago.

Figure 7 shows the distribution of the average stellar mass density (upper panel) and the total dynamical mass (lower panel) as a function of the radius of a sphere around the observer. Data from the UNGC Local volume catalog [41] and the MK11 galaxy group catalog [32], covering distances up to 40 Mpc, were used. The horizontal line in the upper panel corresponds to the global value of the average stellar matter density derived from deep infrared sky surveys [60]. As can be seen from these data, on all scales up to 40 Mpc there is an excess of the local density of luminous matter over its global value.

The behavior of the average density of all matter with distance $\Omega_{\rm m}(D)$ generally follows the distribution of $\Omega_*(D)$. However, in larger volumes with $D > 20$ Mpc, the average density $\Omega_{\rm m}$ is systematically lower than the global value $\Omega_{\rm m} = 0.30$, indicated by the horizontal line. Independent estimates of the virial masses of galaxy groups and clusters, based on data from the catalog [33], also yield an average value of $\Omega_{\rm m} \simeq 0.08 \pm 0.02$ on a scale of ~ 40 Mpc. Various assumptions have been proposed to explain the discrepancy between the local and global estimates of $\Omega_{\rm m}$.

According to [61, 62], the dark matter density profile in galaxy systems may be more extended than that of baryonic matter; in this case, most of the dark matter would be contained in invisible halos surrounding groups and clusters. However, this assumption is contradicted by the observational data from Table 2, which show an approximate equality between the total mass estimates made within volumes with radii R_v and $R_0 \simeq 3.5R_v$.

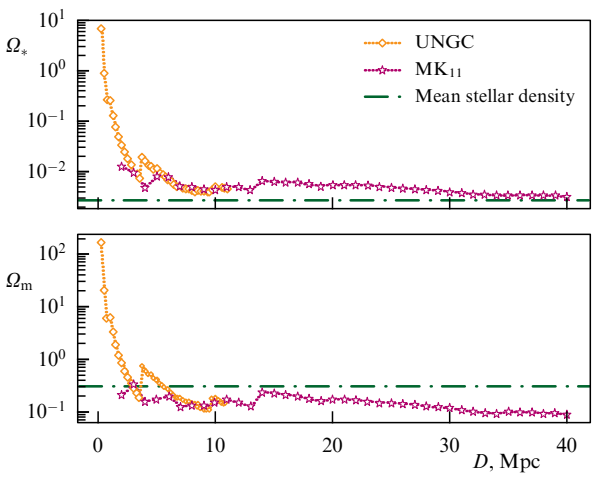

Figure 7. Distributions of the mean stellar density (upper panel) and total matter density (lower panel) as functions of distance from the observer, based on data from the UNGC [41] and MK11 [32] catalogs. Global values of the mean stellar density and total matter density are shown as horizontal lines.

Another explanation suggests that the 80-Mpc diameter region of the Local Universe under consideration does not correspond to the scale of the cosmological 'homogeneity cell.' An observer on Earth could be located within an extended cosmic void, where the average matter density is approximately three times lower than the global density. However, the data shown in the upper panel of Fig. 7 suggest that the broader vicinity of our Galaxy is characterized not by a deficit, but by an excess of local stellar density. Furthermore, galaxy counts extending to deep limits and covering different regions of the sky [63–66] do not provide any convincing evidence for the existence of a vast local void measuring $\sim (100-300)$ Mpc.

A more plausible suggestion is that the bulk of dark matter is distributed in space between groups and clusters, either as a homogeneous dark 'ocean' or as a population of dark attractors with varying masses. The dark ocean hypothesis appears less attractive, since it requires a different type of dark matter, one not subject to Jeans instability.

The existence of dark attractors with masses of $\sim 10^{12}-10^{15} M_\odot$, in which star formation has not occurred, appears more plausible. Weak gravitational lensing can be used to detect them. Analysis of the shapes of distant background galaxies, stretched tangentially relative to a closer attractor (gravilens), makes it possible to determine the coordinates and mass of the attractor. A study of this effect in a 72-square-degree region of the sky, imaged with a wide-field telescope using subsecond seeing, showed [67] that among the three hundred detected gravitational potential peaks, approximately 60% are not associated with visible galaxy clusters. This indicates the possible existence of a population of dark attractors with masses typical of rich galaxy clusters. Weak gravitational lensing is currently being observed in deeper surveys covering a significant portion of the entire sky [14]. Analysis of these data will allow one to determine in the next few years whether isolated massive dark matter clumps exist in the Universe.

Note that a diffuse cloud of galaxies, 'Coma I,' has been discovered in the Local volume, where unusually large motions of dwarf galaxies are observed, reaching 800 km s^{-1}. The perturbed kinematics of this region may be due to the presence of a dark attractor with a mass of $\sim 2 \times 10^{14}\, M_\odot$, located at a distance of ~ 15 Mpc from us [68].

The large-scale structure of the Universe can be roughly divided into three dynamic categories:

(a) virial zones of groups and clusters, where a balance between kinetic and potential energies has been established, and the members of the system have 'forgotten' the initial conditions of their formation;

(b) collapsing regions around virial zones, bounded by zero-velocity spheres with radius R_0; and

(c) the remaining infinitely expanding volume of the general metagalactic field.

The results of numerical simulations of the large-scale structure [69, 70], together with accumulated observational data in the Local volume [71], make it possible to characterize these regions by the parameters presented in Table 3. As can be seen from the first two rows of the table, approximately half of all galaxies and more than 80% of their stellar mass are contained within the virial zones of groups and clusters. Apparently, the main stage of the dynamic evolution of the large-scale structure has already been completed. Moreover, at the present epoch, the virial volumes of groups and clusters occupy only 0.1% of the total volume, and only about 10% of

Table 3. Dynamic regions of the cosmic web.

Parameters	Virialized	Collapsing	Expanding
Proportion of galaxies	54%	20%	26%
Stellar mass	82%	8%	10%
Relative volume	0.1%	5%	95%
Contribution to $\Omega_{\rm m}$	0.06	0.02	0.22

the stellar mass is concentrated within the remaining 95% of the expanding volume. From these figures, which still retain significant uncertainties, it can be estimated that the ratio of dark and stellar matter in the total field outside the virial and collapsing zones around galaxy systems reaches a value of $M_{\rm DM}/M_* \sim 1000$.

6. Conclusions

This brief review outlines the main challenges to the standard cosmological model (ΛCDM), revealed through comparisons between its predictions and observational data obtained in the Local volume of the Universe. Some of these challenges are gradually losing their significance, while others continue to stimulate further development of the theory. In recent years, deep and extensive sky surveys have been planned using large ground-based and orbital telescopes operating across various spectral ranges: the Euclid mission [72], the Roman Space Telescope [73], and the Vera Rubin Observatory [74]. The implementation of these projects will significantly advance our understanding of the nature of the mysterious components of the Universe — dark matter and dark energy. In particular, we will be able to determine whether purely dark massive attractors exist in the space between galaxy clusters.

What will the Universe look like in hundreds of billions of years? The answer depends on the still poorly understood properties of dark matter and dark energy. Numerous studies have already been devoted to dark energy. Different interpretations of its nature are presented in reviews [75, 76]. Progress in understanding this fundamental physical substance, permeating the entire space of the visible Universe, has not yet led to a definite conclusion. It should be noted that the classical Friedmann equation without the Λ term and with $\Omega_{\rm m} = 1$ describes an oscillatory cosmological model, in which cycles of expansion and contraction of the Universe can alternate indefinitely. The inclusion of the Λ term radically changes the situation. Acting as a universal repulsive force, dark energy causes galaxies to recede from one another, leads to an irreversible decrease in the average density of baryonic matter, increases entropy, and results in the structural degradation of the Universe. However, this scenario may prove to be oversimplified if the space containing black holes possesses a complex topology and if new, unexpected properties of dark energy are discovered in the future.

Acknowledgments. The author thanks D.I. Makarov, V.E. Karachentseva, E.I. Kaisina, O.G. Kashibadze, and S.S. Kaisin for their collaboration. This work was supported by the Russian Science Foundation (grant no. 24-12-00277).

References

1. Vikhlinin A A et al. *Phys. Usp.* **57** 317 (2014); *Usp. Fiz. Nauk* **184** 339 (2014)
2. Gross M A K et al. *Mon. Not. R. Astron. Soc.* **301** 81 (1998)
3. Klypin A et al. *Astrophys. J.* **516** 530 (1999)
4. Knollmann S R, Knebe A *Astrophys. J. Suppl.* **182** 608 (2009)
5. Moore B et al. *Astrophys. J.* **524** L19 (1999)
6. Klypin A et al. *Astrophys. J.* **522** 82 (1999)
7. Kim S Y, Peter A H G, Hargis J R *Phys. Rev. Lett.* **121** 211302 (2018)
8. Kroupa P, Theis C, Boily C M *Astron. Astrophys.* **431** 517 (2005)
9. Ibata R A et al. *Nature* **493** 62 (2013)
10. Pawlowski M S, Kroupa P, Jerjen H *Mon. Not. R. Astron. Soc.* **435** 1928 (2013)
11. Martínez-Delgado D et al. *Astron. Astrophys.* **652** A48 (2021)
12. Dupuy A et al. *Mon. Not. R. Astron. Soc.* **516** 4576 (2022)
13. Aghanim N et al. (Planck Collab.) "Planck 2018 results. VI. Cosmological parameters" *Astron. Astrophys.* **641** A6 (2020)
14. Anbajagane D et al. *Open J. Astrophys.* **8** 46161 (2025) DOI:10.33232/001c.146161; arXiv:2502.17677
15. Kourkchi E et al. *Astrophys. J.* **902** 145 (2020)
16. Riess A G et al. *Astrophys. J. Lett.* **934** L7 (2022)
17. Riess A G et al. *Astron. J.* **861** 126 (2018)
18. Keenan R C, Barger A J, Cowie L L *Astrophys. J.* **775** 62 (2013)
19. Böhringer H, Chon G, Collins C A *Astron. Astrophys.* **633** A19 (2020)
20. Fukugita M, Peebles P J E *Astrophys. J.* **616** 643 (2004)
21. Spergel D N et al. *Astrophys. J. Suppl.* **170** 377 (2007)
22. Bahcall N A et al. *Astrophys. J.* **541** 1 (2000)
23. Popov S B, Postnov K A, Pshirkov M S *Phys. Usp.* **61** 965 (2018); *Usp. Fiz. Nauk* **188** 1063 (2018)
24. Macquart J-P et al. *Nature* **581** 391 (2020)
25. Yang K B, Wu Q, Wang F Y *Astrophys. J. Lett.* **940** L29 (2022)
26. Mandelbaum R et al. *Mon. Not. R. Astron. Soc.* **368** 715 (2006)
27. Zwicky F *Astrophys. J.* **86** 217 (1937)
28. Zasov A V et al. *Phys. Usp.* **60** 3 (2017); *Usp. Fiz. Nauk* **187** 3 (2017)
29. van Uitert E et al. *Astron. Astrophys.* **534** A14 (2011)
30. Vennik J *Tartu Astron. Obs. Publ.* (73) 1 (1984)
31. Tully R B *Astrophys. J.* **321** 280 (1987)
32. Makarov D, Karachentsev I *Mon. Not. R. Astron. Soc.* **412** 2498 (2011)
33. Kourkchi E, Tully R B *Astrophys. J.* **843** 16 (2017)
34. Peebles P J E *Astrophys. J.* **155** 393 (1969)
35. Doroshkevich A G *Astrophysics* **6** 320 (1970); *Astrofizika* **6** 581 (1970)
36. White S D M *Astrophys. J.* **286** 38 (1984)
37. Antipova A V, Makarov D I, Bizyaev D V *Astrophys. Bull.* **76** 248 (2021); *Astrofiz. Byull.* **76** 306 (2021)
38. Karachentsev I D, Zozulia V D *Mon. Not. R. Astron. Soc.* **522** 4740 (2023)
39. Kraan-Korteweg R C, Tammann G A *Astron. Nachr.* **300** 181 (1979)
40. Karachentsev I D et al. *Astron. J.* **12** 2031 (2004)
41. Karachentsev I D, Makarov D I, Kaisina E I *Astron. J.* **145** 101 (2013)
42. Abazajian K N et al. *Astrophys. J. Suppl.* **182** 543 (2009)
43. Dey A et al. *Astron. J.* **157** 168 (2019)
44. Donley J L et al. *Astron. J.* **129** 220 (2005)
45. Haynes M P et al. *Astron. J.* **142** 170 (2011)
46. Zhang C-P et al. *Sci. China Phys. Mech. Astron.* **67** 219511 (2024)
47. Huchtmeier W K et al. *Astron. Astrophys. Suppl. Ser.* **141** 469 (2000)
48. Huchtmeier W K, Karachentsev I D, Karachentseva V E *Astron. Astrophys.* **377** 801 (2001)
49. Huchtmeier W K, Karachentsev I D, Karachentseva V E *Astron. Astrophys.* **401** 483 (2003)
50. Karachentsev I D, Chazov M I, Kaisin S S *Mon. Not. R. Astron. Soc.* **537** L21 (2025)
51. Kaisina E I et al. *Astrophys. Bull.* **67** 115 (2012); *Astrofiz. Byull.* **67** (1) 120 (2012)
52. Karachentsev I D, Kudrya Yu N *Astron. J.* **148** 50 (2014)
53. Dolgosheeva P, Makarov D, Libeskind N *Astron. Astrophys.* **698** L8 (2025)

54. Shamir L *Mon. Not. R. Astron. Soc.* **516** 2281 (2022)
55. Karachentsev I D et al. *Mon. Not. R. Astron. Soc.* **393** 1265 (2009)
56. Kashibadze O G, Karachentsev I D *Astron. Astrophys.* **609** A11 (2018)
57. Karachentsev I D et al. *Astrophys. J.* **782** 4 (2014)
58. Karachentsev I D et al. *Astrophys. J.* **858** 62 (2018)
59. Makarov D et al. *Astron. Astrophys.* **698** A178 (2025)
60. Driver S P et al. *Mon. Not. R. Astron. Soc.* **427** 3244 (2012)
61. Rines K, Diaferio A *Astron. J.* **132** 1275 (2006)
62. Masaki S, Fukugita M, Yoshida N *Astrophys. J.* **746** 38 (2012)
63. Djorgovski S et al. *Astrophys. J. Lett.* **438** L13 (1995)
64. Bershady M A, Lowenthal J D, Koo D C *Astrophys. J.* **505** 50 (1998)
65. Totani T et al. *Astrophys. J.* **559** 592 (2001)
66. Huang J-S et al. *Astron. Astrophys.* **368** 787 (2001)
67. Shan H et al. *Astrophys. J.* **748** 56 (2012)
68. Karachentsev I D, Nasonova O G, Courtois H M *Astrophys. J.* **743** 123 (2011)
69. Cautun M et al. *Mon. Not. R. Astron. Soc.* **441** 2923 (2014)
70. Nuza S E et al. *Mon. Not. R. Astron. Soc.* **445** 988 (2014)
71. Karachentsev I D *Astrophys. Bull.* **67** 123 (2012); *Astrofiz. Byull.* **67** (2) 129 (2012)
72. Enia A et al. (Euclid Collab.) *Astron. Astrophys.* **691** A175 (2024)
73. Wang K et al. *Mon. Not. R. Astron. Soc.* **546** staf2253 (2026) DOI:10.1093/mnras/staf2253; arXiv:2501.16139
74. Rubin D et al., arXiv:2506.04327; *Astrophys. J.*, submitted
75. Chernin A D *Phys. Usp.* **51** 253 (2008); *Usp. Fiz. Nauk* **178** 267 (2008)
76. Lukash V N, Rubakov V A *Phys. Usp.* **51** 283 (2008); *Usp. Fiz. Nauk* **178** 301 (2008)